A simple example

Evensen (1992)

Model: 1-D linear advection equation in a periodic domain:

$$\frac{\partial F}{\partial t} + c\frac{\partial F}{\partial x} = 0$$

- Truth = sinusoid traveling left to right
- perfect obs at x=5 and x=20, every 5 time steps. Error variance $2\times$ worse at x=20.
- background is $F = 0$
- background error variance is 1, correlation function $\sim \exp[-(r/r_c)^2]$

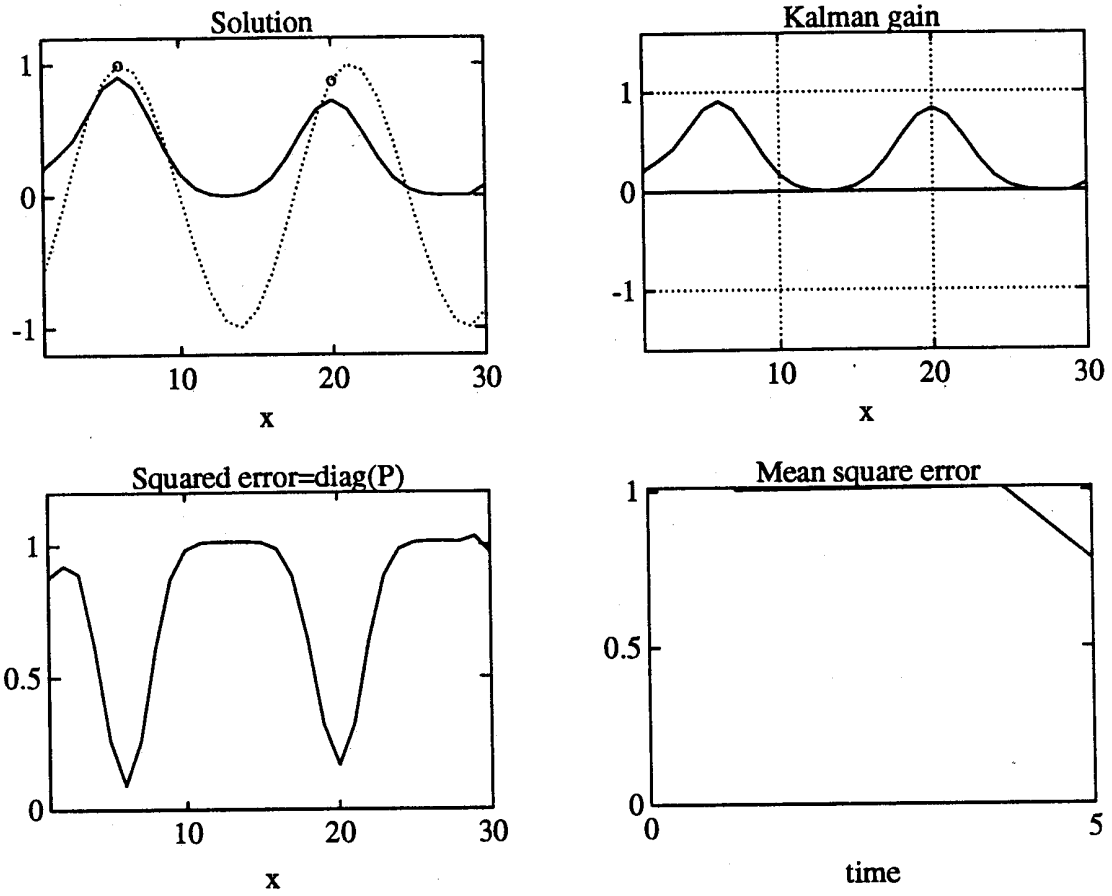

Fig. 1. Solution of the advection equation after one update with the Kalman filter. The upper left plot shows the true solution as a dotted line and the estimated solution as the solid line. The circles are the values of the measurements. The lower left plot shows the estimated error variance for each grid point (the diagonal elements of P). The Kalman gain influence (columns of K) are shown in the upper right plot. The lower right plot shows the time history of the mean square error, i.e., the normalized trace of P.

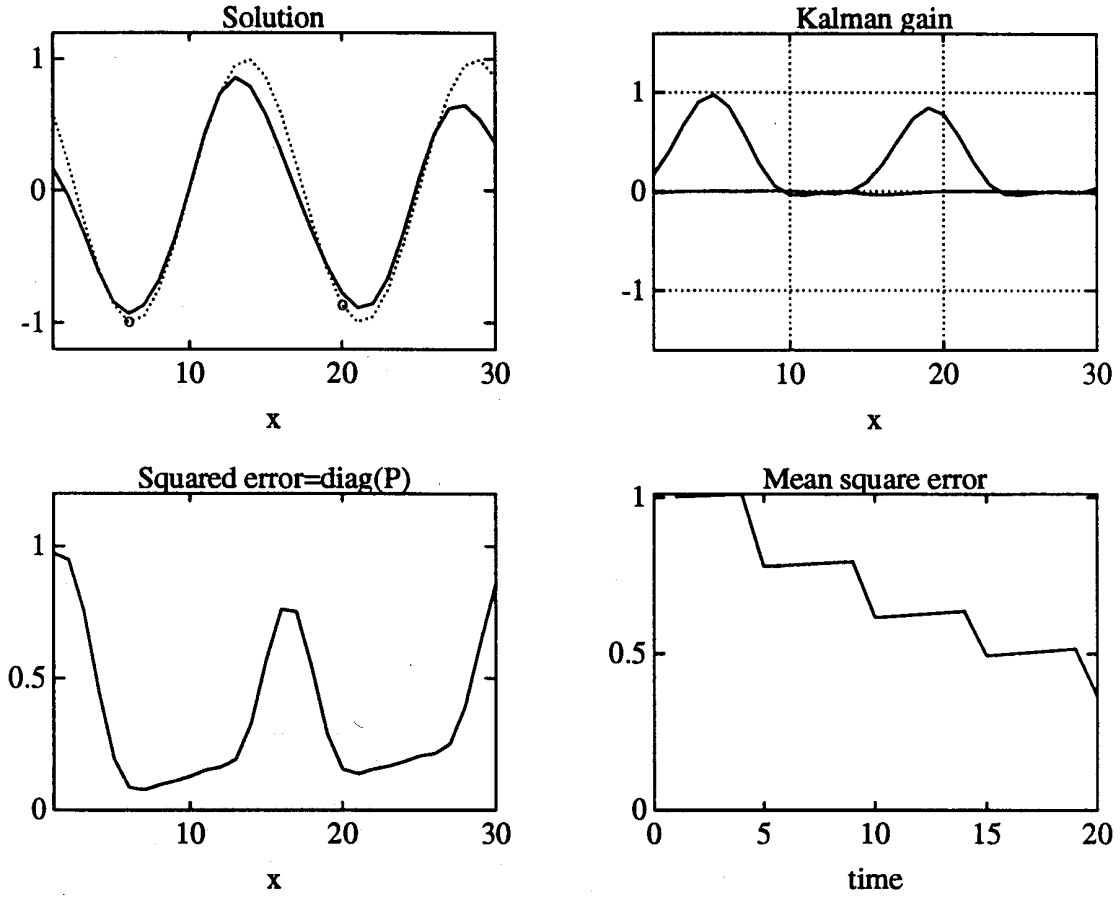

Fig. 2. The same as Figure 1 but after four updates with the Kalman filter.

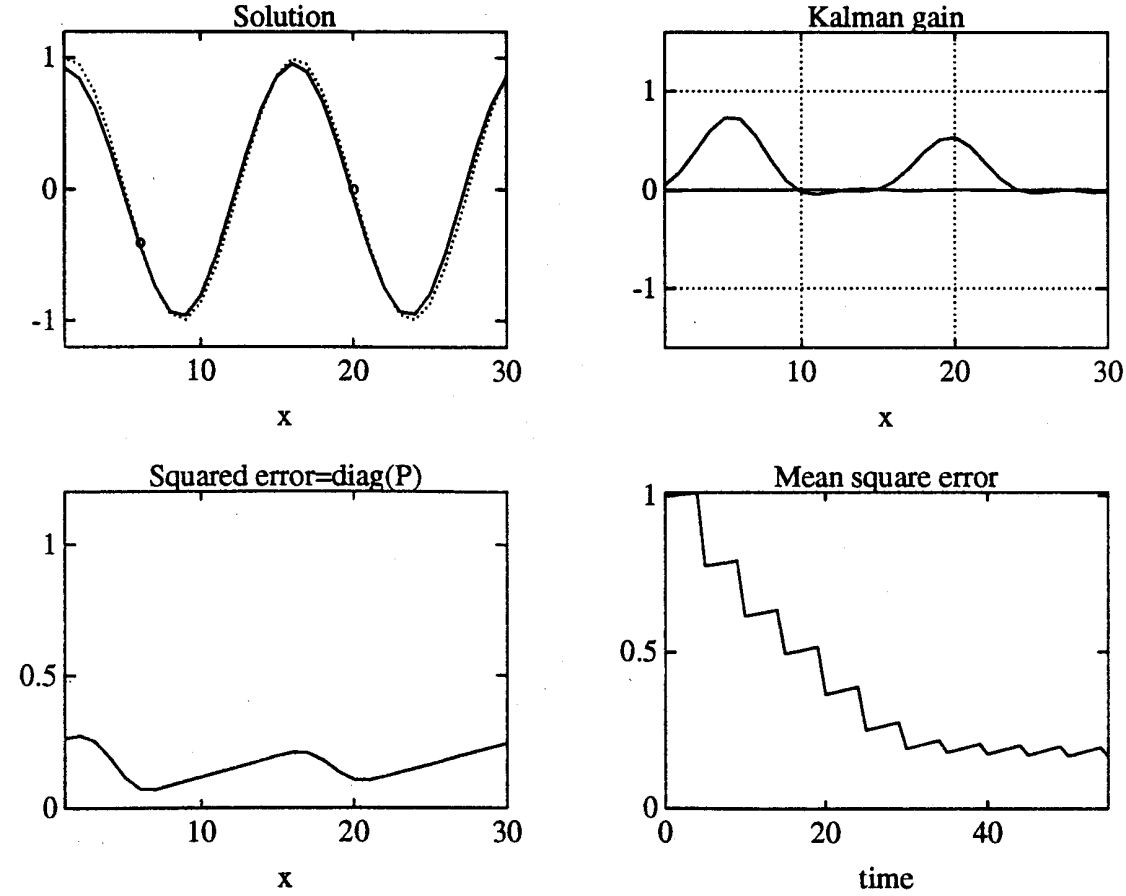

Fig. 3. The same as Figure 1 but after 11 updates with the Kalman filter. Evensen (1992)

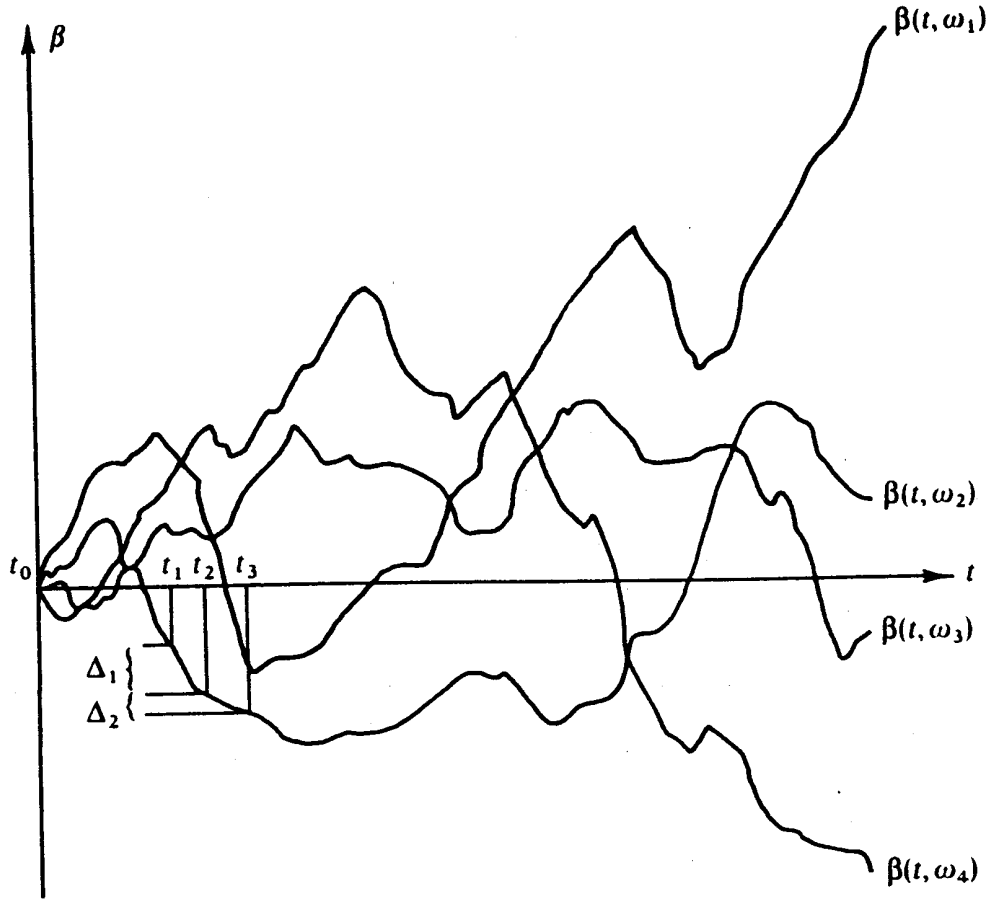

FIG. 4.8 Samples from a Brownian motion process.

Maybeck (1979)

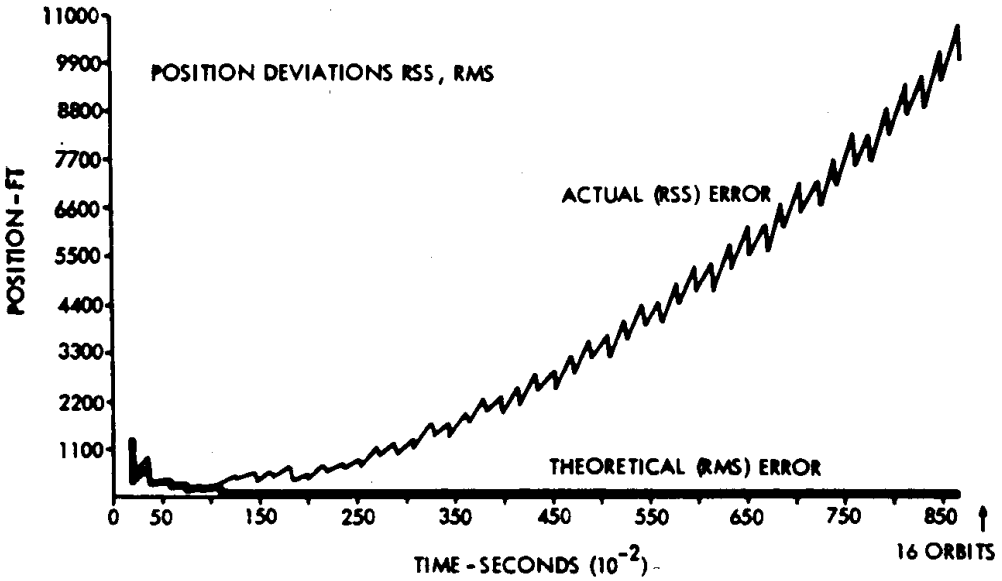

Fig. 1. Kalman filter divergence caused by 25% error in drag acceleration.

Schlee et al. (1967)

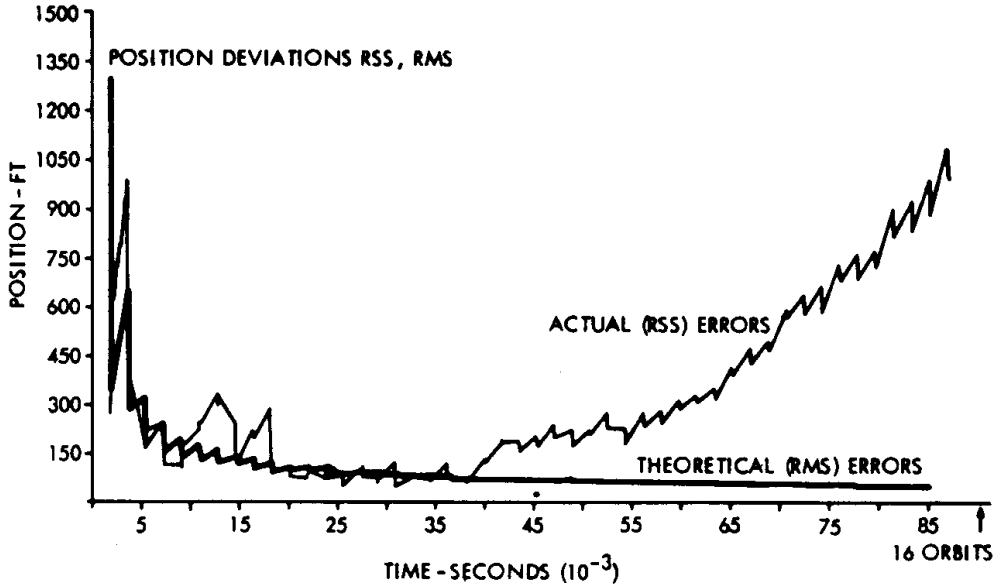

Fig. 2 Divergence of the Kalman filter caused by computional errors resulting from single precision arithmetic (IBM 7090).

Schlee et al. (1967)

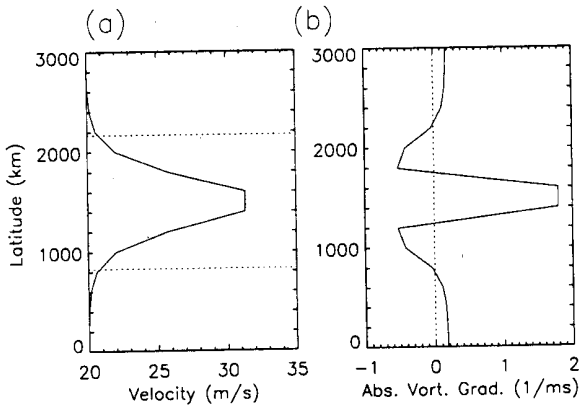

Fig. 1. Meridionally-dependent unstable Bickley jet (a) and its corresponding absolute vorticity gradient (b), scaled by 10^{10}.

Cohn and Todling (1996)

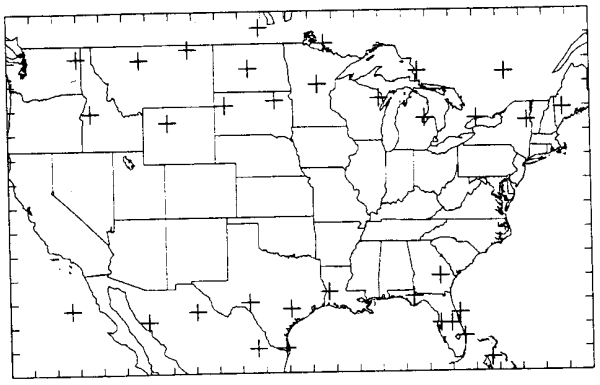

Fig. 2. Observation network consisting of 33 radiosondes observing outside the jet of Fig. 1a.

Cohn and Todling (1996)

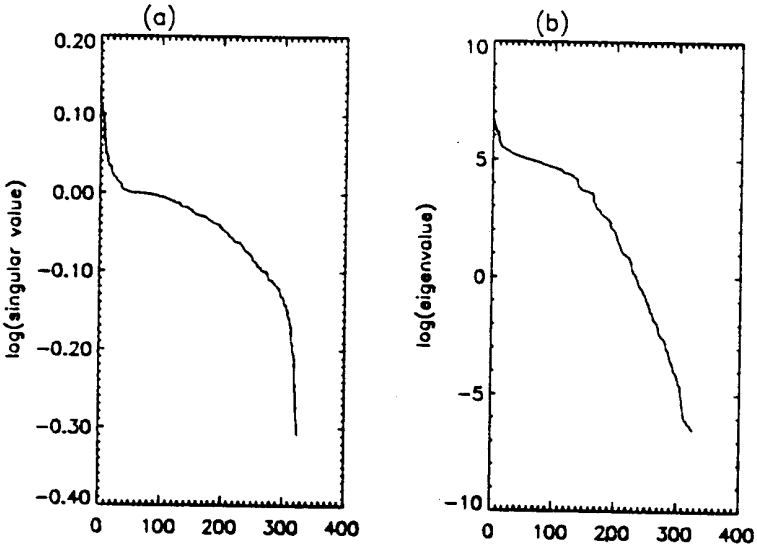

Figure 1: Spectra of singular values of the 12–hour propagator (a) and eigenvalues of the KF forecast error covariance at day 10 (b).

Cohn and Todling (1995)

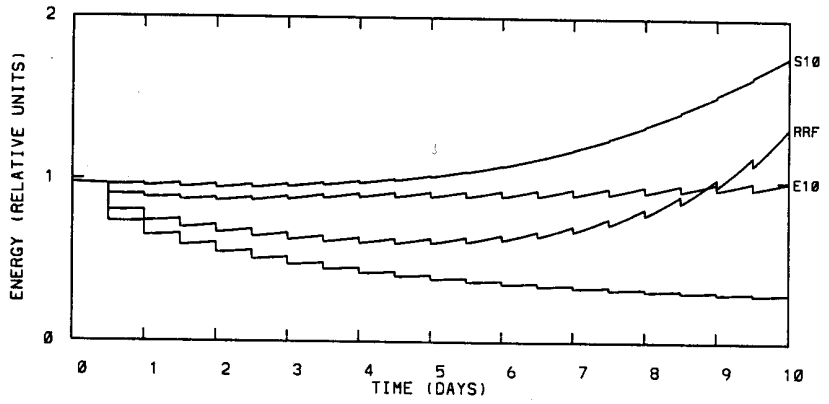

FIGURE 4. ERMS forecast/analysis error in the total energy for a 10-day assimilation period, with a perfect, barotropically unstable model, using the KF (lowest unlabeled curve) and three approximations: reduced resolution filter (RRF) on a grid with dimensions 13×12, in contrast to the full resolution of 25×16; partial singular value decomposition filter (S10) including the first 10 singular modes of the dynamics within each 12–hour period; and a partial eigendecomposition filter (E10), including the first 10 eigenmodes of the propagated error covariance structure during each 12–hour period. Error growth between consecutive analysis times is solely due to the presence of unstable modes. Same as Fig. 10 in Cohn & Todling (1996).

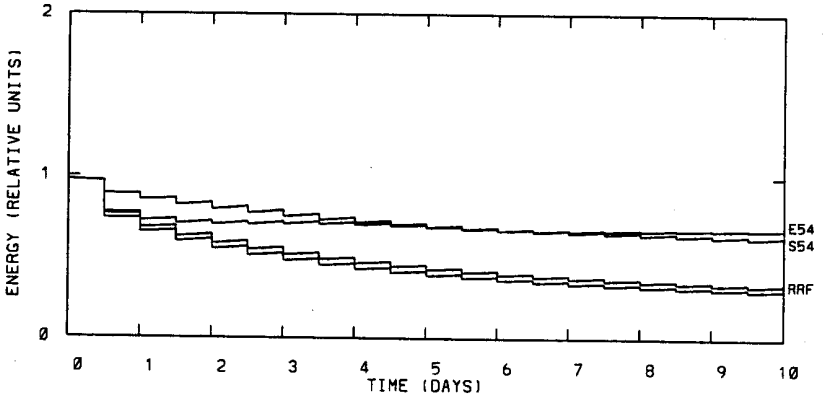

FIGURE 5. Same as in Fig. 4, but for RRF at 13×16 resolution, the PSF with 54 singular modes (S54) and the PEF with 54 eigenmodes (E54). The bottom curve is for the KF result. Same as Fig. 11 in Cohn & Todling (1996).

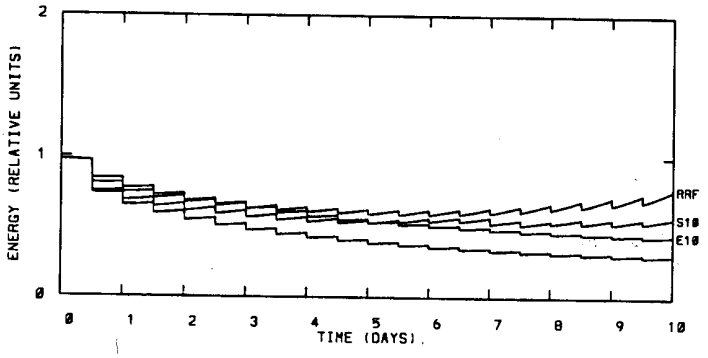

Fig. 12. As in Fig. 10, but with adaptively estimated trailing error covariance magnitude. The bottom curve is for the KF result.

Cohn and Todling (1996)

Highly nonlinear dynamics

Lorenz (1963) equations

$$\begin{aligned} \dot{x} &= \sigma(y - x) \\ \dot{y} &= \rho x - y - xz \\ \dot{z} &= xy - \beta z \end{aligned}$$

for σ=10, ρ=28, β=8/3.

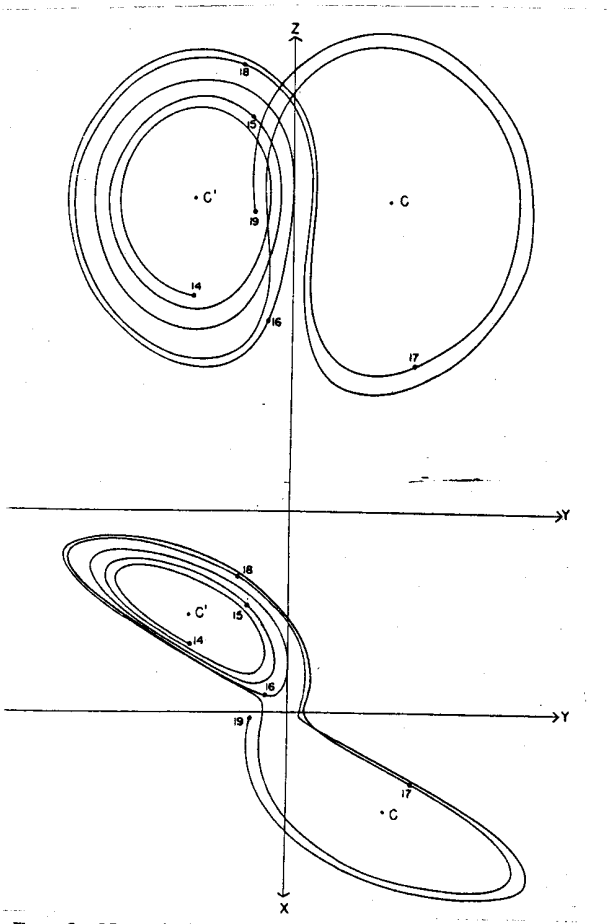

FIG. 2. Numerical solution of the convection equations. Projections on the X-Y-plane and the Y-Z-plane in phase space of the segment of the trajectory extending from iteration 1400 to iteration 1900. Numerals "14," "15," etc., denote positions at iterations 1400, 1500, etc. States of steady convection are denoted by C and C'.

Lorenz (1963)

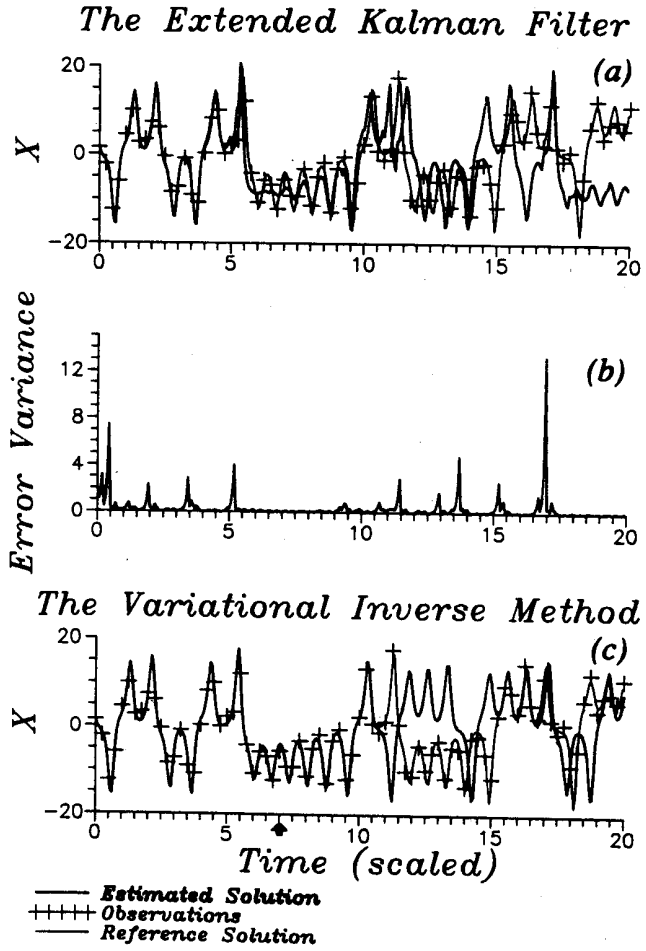

FIG. 3. Results of filtering and smoothing experiments for the Lorenz model. (a) Estimate of the state variable X by the extended Kalman filter (EKF). Thin line: reference solution; plus signs: simulated observations; heavy line: filtered output. (b) Estimated error variance from the EKF corresponding to panel (a). (c) Similar to (a) but estimate is by calculation of initial data to minimize difference between solution and observations. Minimization was carried out on observations from $t = 0$ through $t = 7$ (see arrow). Beyond $t = 7$, the heavy line represents the solution to the Lorenz equations with the calculated initial data.

Miller et al. (1994)

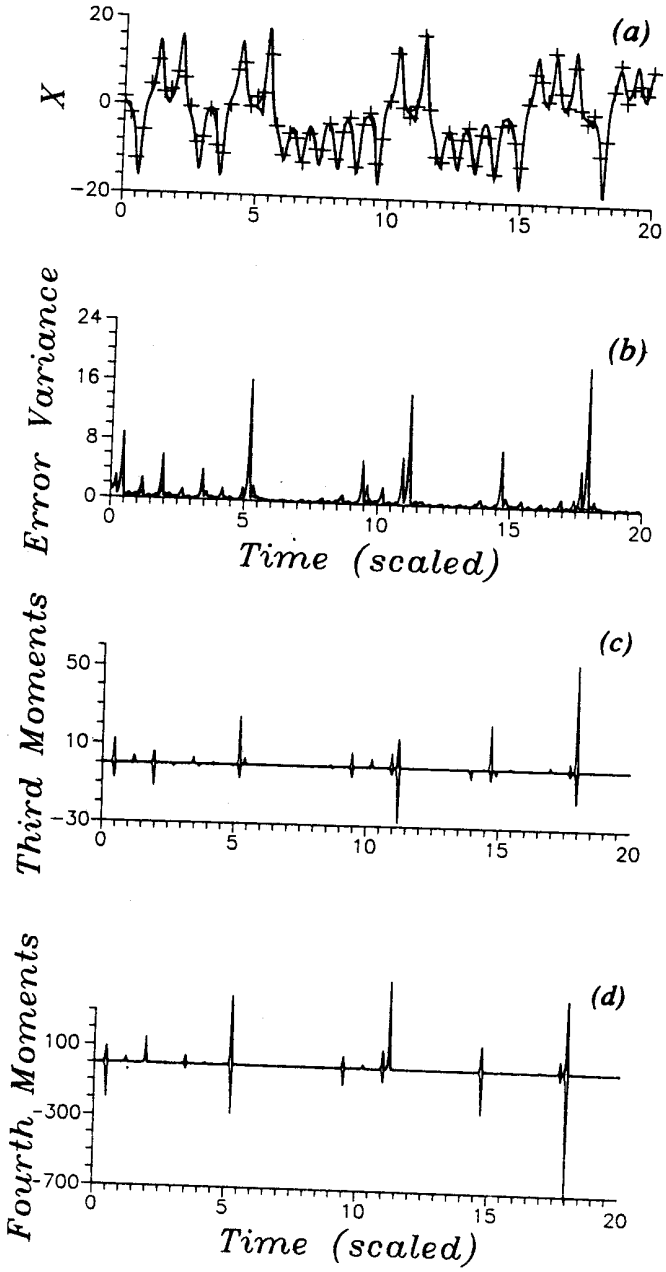

FIG. 7. Results of modified EKF with third- and fourth-order moments calculated explicitly. (a) Estimates of the variable X. Heavy line: filtered solution; thin line: reference solution; "+" signs: simulated observations. (b) Estimated error variances. Heavy line: Estimated error variance for X; thin line: estimated error variance from ordinary EKF. (c) Calculated third error moments. Heavy line: $\Theta(1, 1, 1)$; thin line: $\Theta(1, 3, 3)$. (d) Calculated fourth error moments. Heavy line: $\Gamma(1, 1, 1, 1)$; thin line: $\Gamma(1, 1, 2, 3)$.

Miller et al. (1994)

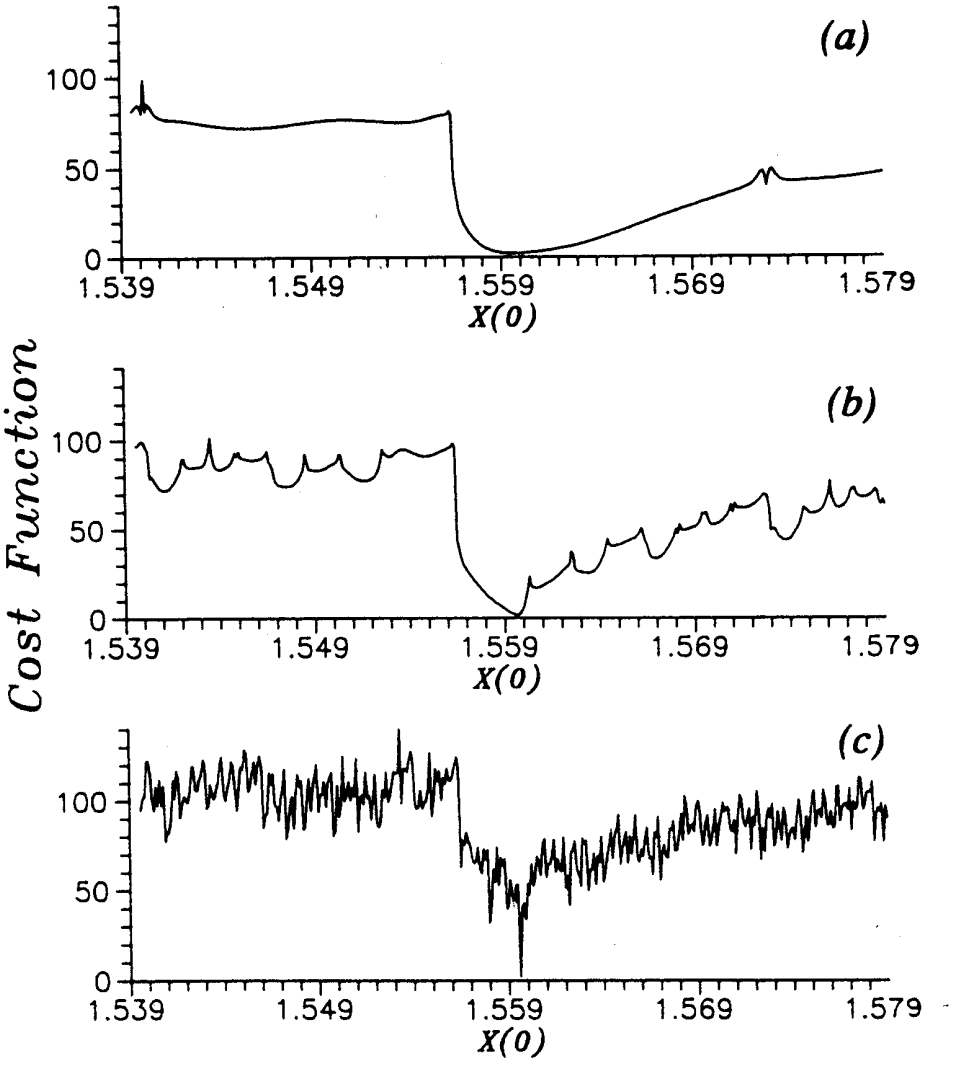

FIG. 6. Values of cost function as a function of initial X, with initial Y and Z held constant, in the neighborhood of the initial values used in calculating the reference solution. (a) Cost function, i.e., mean-square deviation of model solution with given initial data from "observed" values, where observations up to $t = 8$ are considered. (b) As in (a) but for observations up to $t = 10$. (c) As in (a) but for observations up to $t = 15$.

Miller et al. (1994)

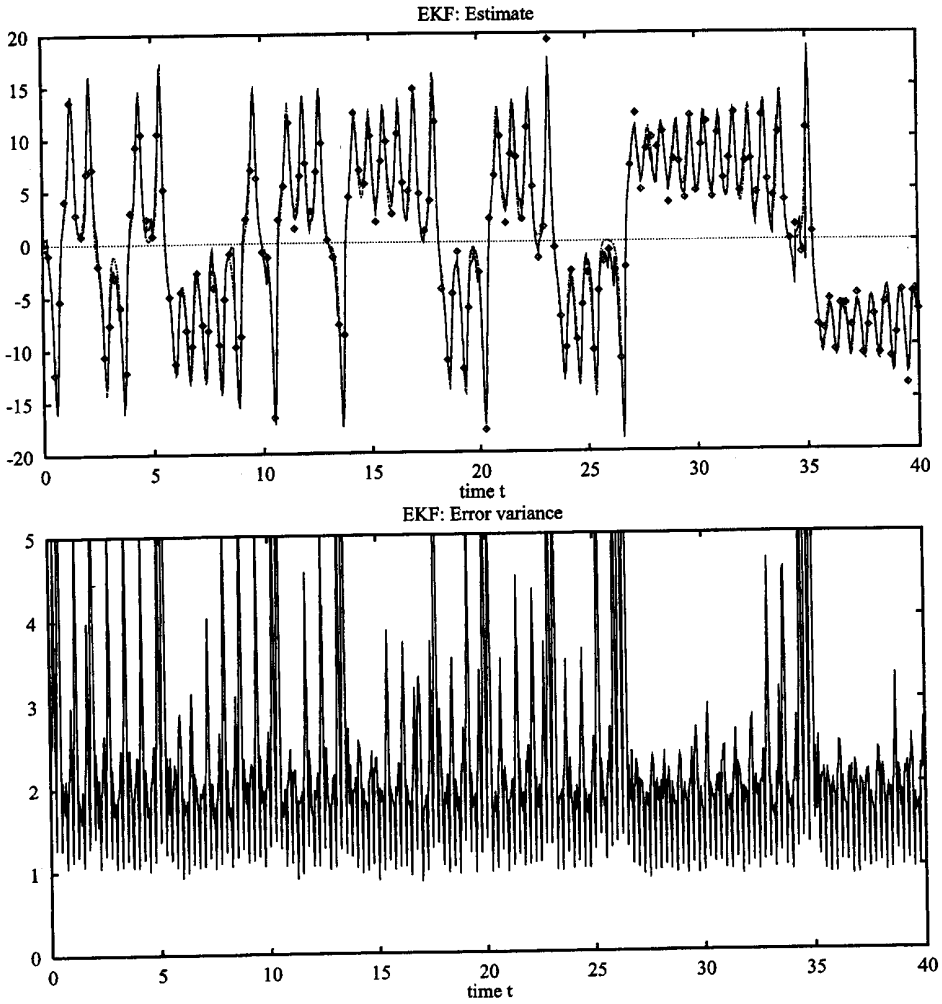

FIG. 3. Experiment A (ensemble Kalman filter): The inverse estimate for x (upper) and the corresponding error variance estimate (lower).

Evensen (1997)

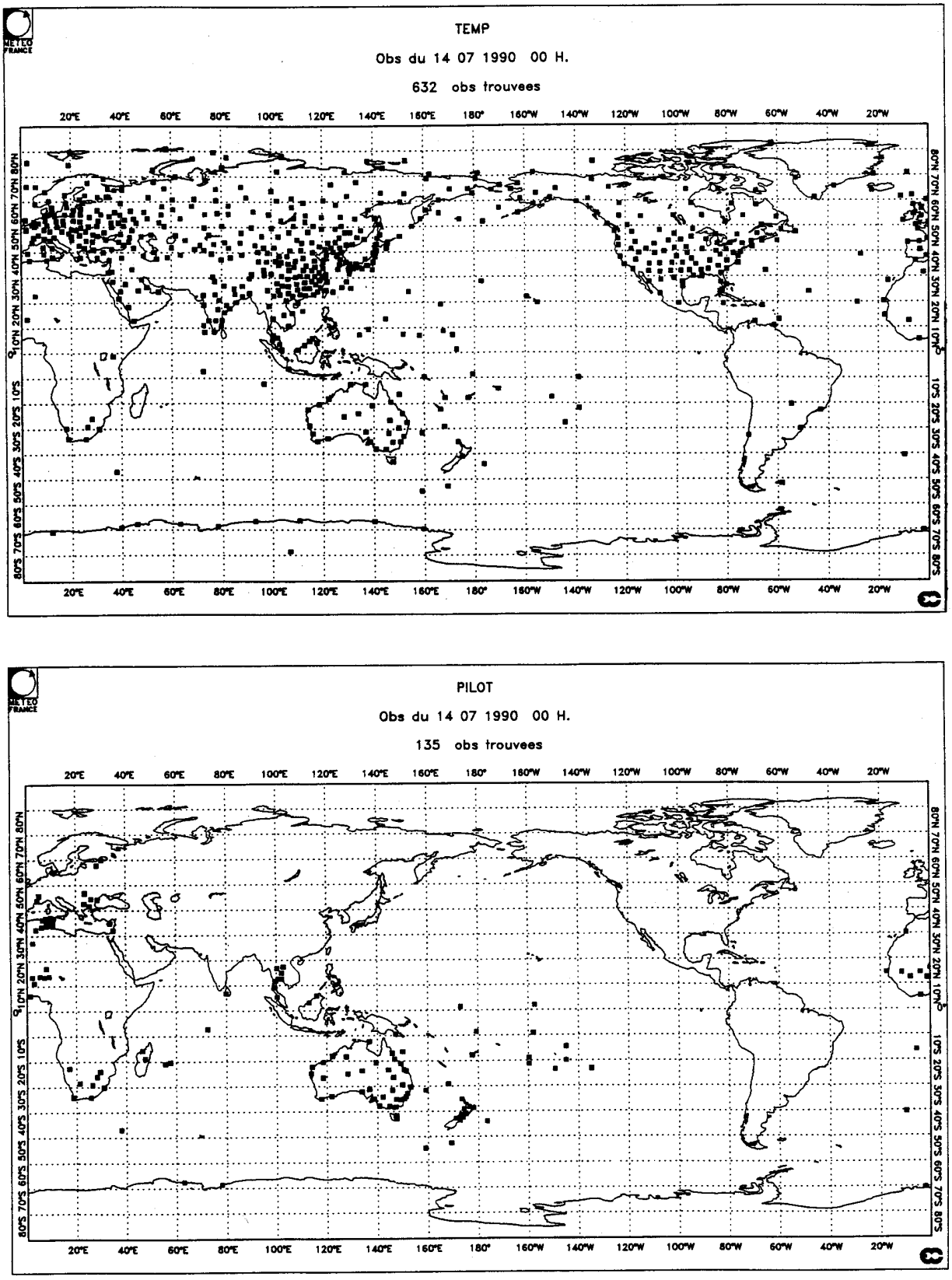

FIG. 1. Typical radiosonde network at 0000 UTC for TEMP and PILOT. This network is assumed to be the same every 6 h.

Gauthier et al. (1993)

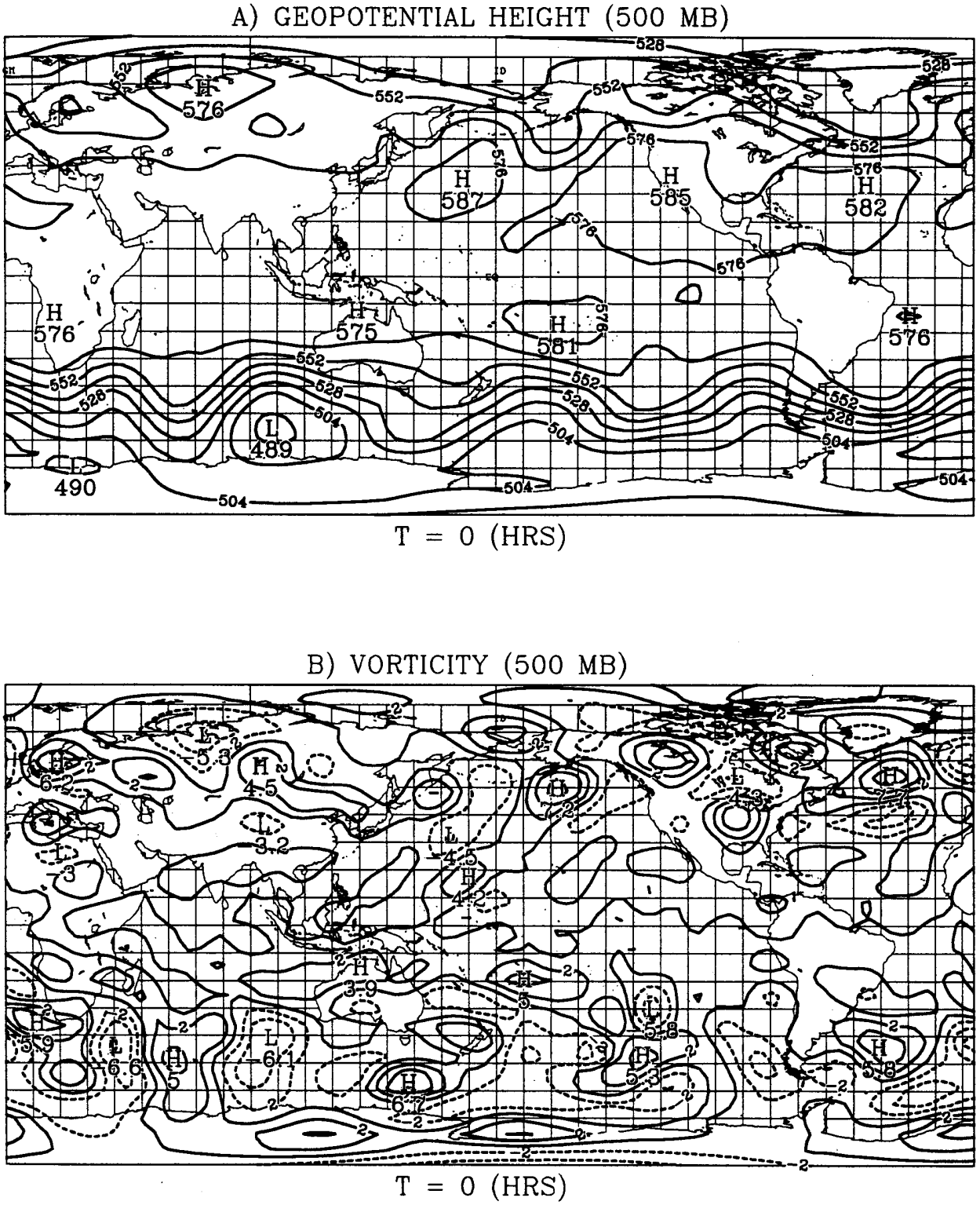

FIG. 2. Initial conditions on 14 July 1990: (a) geopotential field and (b) vorticity field.

Gauthier et al. (1993)

-A-

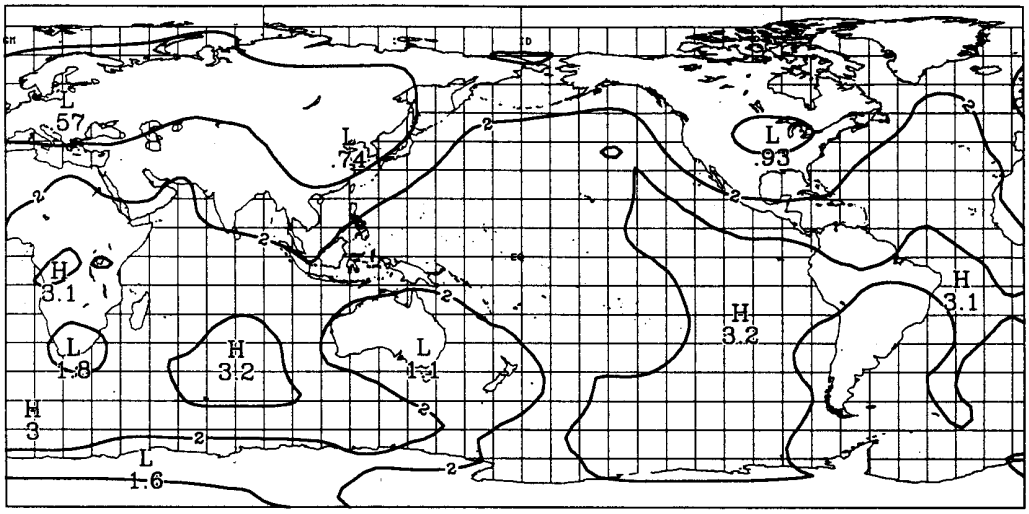

T = 0 (HRS)

-B-

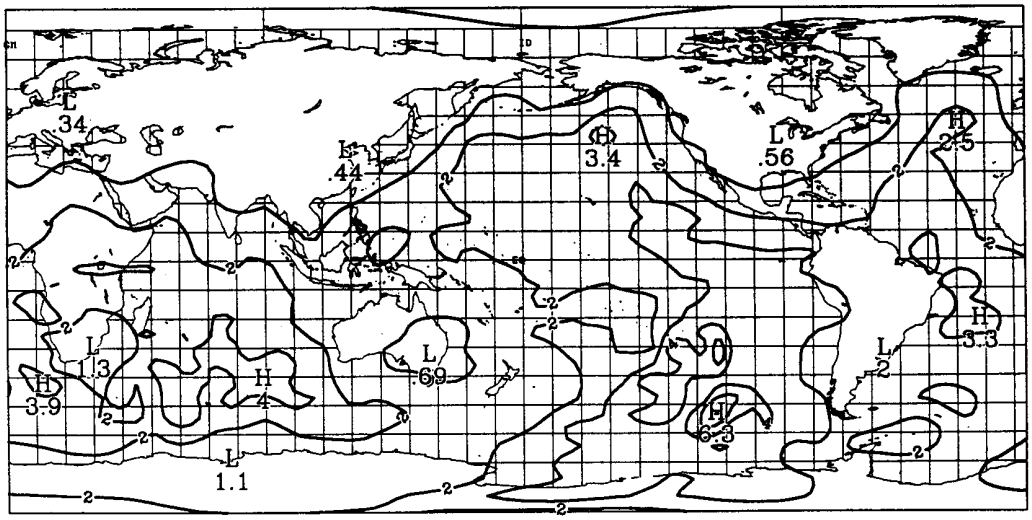

T = 12 (HRS)

-C-

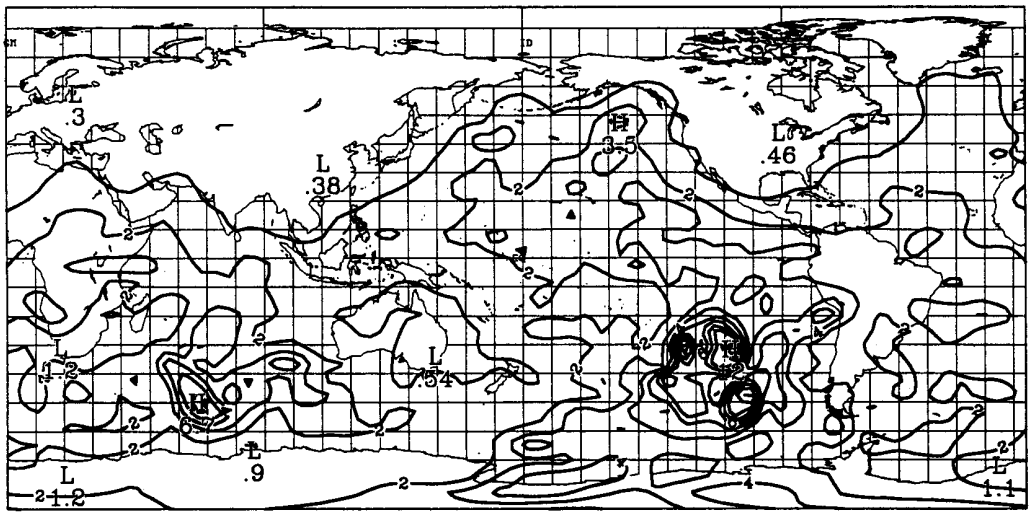

T = 24 (HRS)

FIG. 3. Analysis error variance resulting from an assimilation with the extended Kalman filter: (a) $t = 0$ h, (b) 12 h, and (c) 24 h. Units used are $1 \times 10^{-12}\ s^{-2}$, with contour levels of 1 unit, and the characteristic length of the first-guess error is 1200 km.

Gauthier et al. (1993)

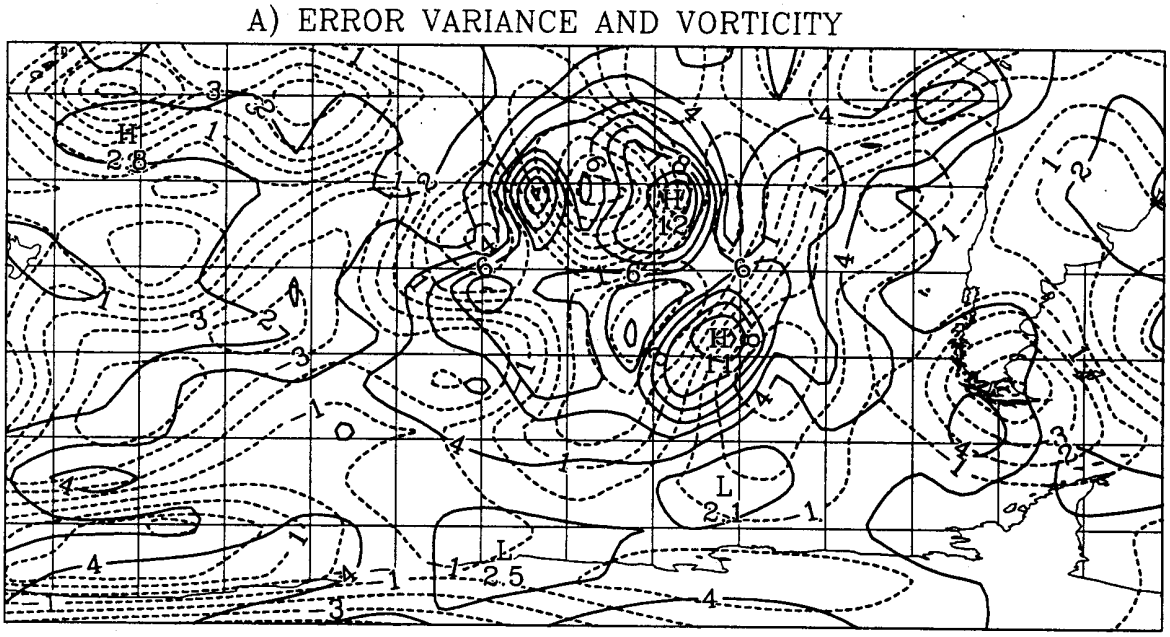

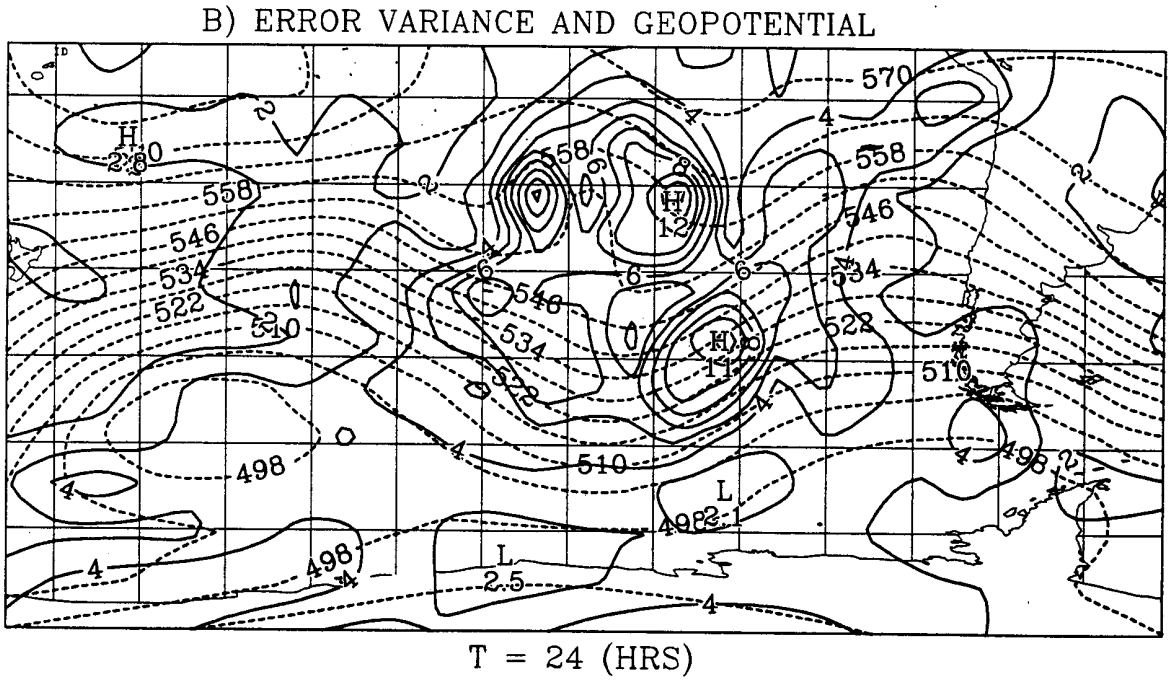

FIG. 4. Analysis error variance field at t = 24 h superposed over (a) the vorticity field and (b) the geopotential field. The domain is a close-up of the region west of South America.

Gauthier et al. (1993)

Evaluation of CH_4 budget in Europe

Zhang and Heemink (1996)

- EUROS - Eulerian dispersion model
- augment state vector to estimate emissions:

$$\begin{bmatrix} X_{k+1} \\ S_{k+1} \end{bmatrix} = \begin{bmatrix} \mathbf{M}_k & \mathbf{G} \\ 0 & (1-\epsilon)\mathbf{I} \end{bmatrix} \begin{bmatrix} X_k \\ S_k \end{bmatrix} + \begin{bmatrix} \mathbf{B} \\ 0 \end{bmatrix} S_B + \begin{bmatrix} \Gamma_s & 0 \\ 0 & \Gamma_e \end{bmatrix} \begin{bmatrix} w_k^s \\ w_k^e \end{bmatrix}$$

$$Y_k = \begin{bmatrix} \mathbf{H} & 0 \end{bmatrix} \begin{bmatrix} X_k \\ S_k \end{bmatrix} + v_k$$

- $S_B = S_{\text{true}} + \gamma S_B$, $\gamma = \pm\ 20\ \%$
- Reduced-Rank Square Root Kalman Filter (Verlaan and Heemink 1995)
- N=2885, reduced rank=50

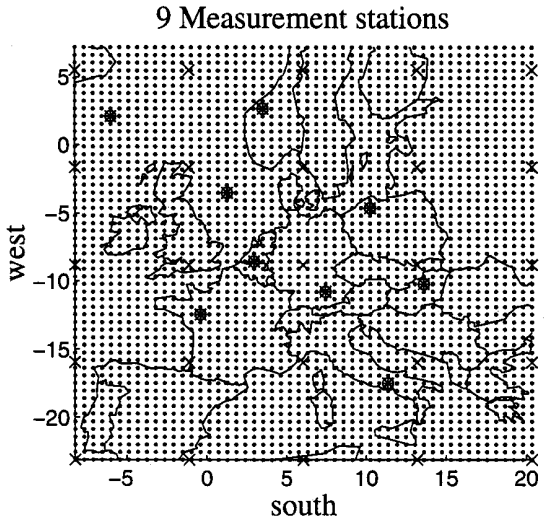

Figure 2: "." Model grid G_m; "x" noise grid G_w; "$*$" measurement stations.

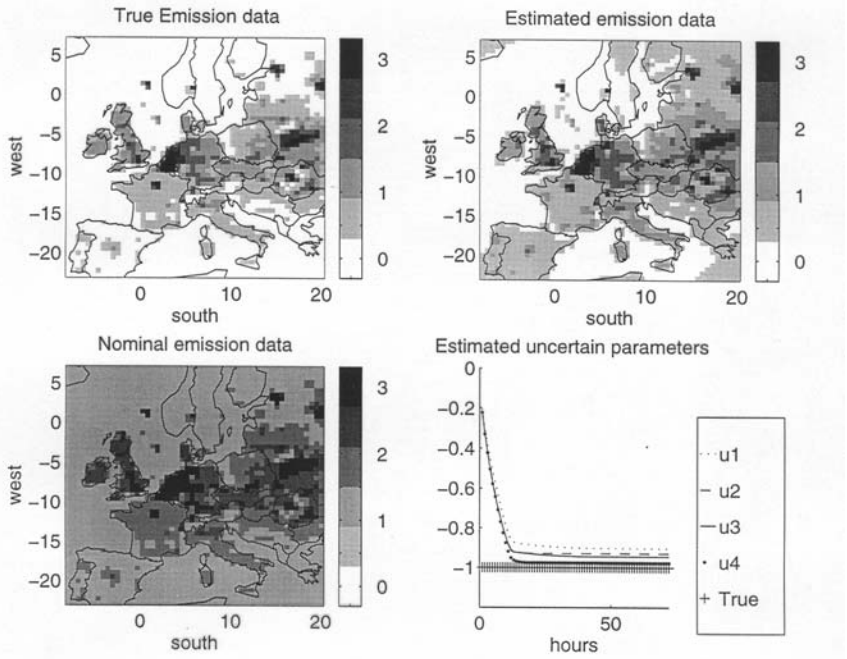

Figure 6: Results of the smoother.
Zhang and Heemink (1996)

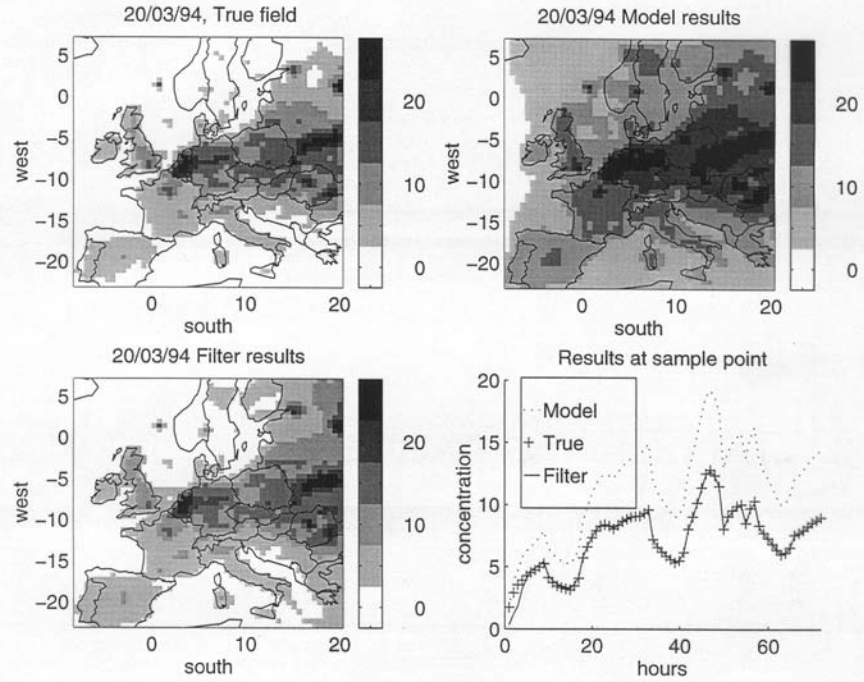

Figure 7: Filter results of using smoother.
Zhang and Heemink (1996)